

Structure, Dynamics, and Energetics of siRNA–Cationic Vector Complexation: A Molecular Dynamics Study

Defang Ouyang,^{†,‡} Hong Zhang,[‡] Dirk-Peter Herten,[§] Harendra S. Parekh,^{*,†} and Sean C. Smith^{*,‡}

School of Pharmacy and Centre for Computational Molecular Science, Australian Institute of Bioengineering and Nanotechnology, The University of Queensland, Brisbane, QLD 4072, Australia, and BIOQUANT/Cellnetworks, Universität Heidelberg, Im Neuenheimer Feld 267, 69120 Heidelberg, Germany

Received: December 16, 2009; Revised Manuscript Received: June 1, 2010

The design and synthesis of safe and efficient nonviral vectors for gene delivery has attracted significant attention in recent years. Previous experiments have revealed that the charge density of a polycation (the carrier) plays a crucial role in complexation and the release of the gene from the complex in the cytosol. In this work, we adopt an atomistic molecular dynamics simulation approach to study the complexation of short strand duplex RNA with six cationic carrier systems of varying charge and surface topology. The simulations reveal detailed molecular-level pictures of the structures and dynamics of the RNA–polycation complexes. Estimates for the binding free energy indicate that electrostatic contributions are dominant followed by van der Waals interactions. The binding free energy between the 8⁺ polymers and the RNA is found to be larger than that of the 4⁺ polymers, in general agreement with previously published data. Because reliable binding free energies provide an effective index of the ability of the polycationic carrier to bind the nucleic acid and also carry implications for the process of gene release within the cytosol, these novel simulations have the potential to provide us with a much better understanding of key mechanistic aspects of gene–polycation complexation and thereby advance the rational design of nonviral gene delivery systems.

1. Introduction

Gene therapy is a promising and rapidly developing medical approach, which aims to cure diseases of genetic origin by correcting the over- or underexpression of genes. Although significant progress has been made, this strategy is still hampered by the lack of effective and safe vectors for gene delivery. In general, in order for a gene to efficiently transfect a host cell population, it must first overcome five major barriers *in vivo*.^{1–3} The first is that a gene complexed with the carrier must overcome extracellular physical and biochemical degradation to reach target cells intact.⁴ Transfer into and passing through the cell membrane is the next hurdle.⁵ After they translocate across the cell membrane, complexes generally enter the endosomal–lysosomal pathway.³ The pH of the endosomal environment then rapidly decreases until a pH \sim 4 is reached, which then triggers fusion of the now “late-endosomes” with lysosomes that release a barrage of degradative enzymes.^{2,3} If timely escape from the endosome is achieved, release of the gene from its vector is the penultimate step prior to the migration of genes across the nuclear membrane and the incorporation into the genome of the host cell. A significant intracellular hurdle and rate-limiting step in gene delivery is the dissociation of the gene from its vector, which can be impeded by the underlying high affinity that exists between cationic vector and anionic gene.^{6,7} The final obstacle for gene transfer of plasmid DNA (pDNA) is migration across the nuclear membrane and entry

into the nucleus. In the case of RNA interference (gene silencing using siRNA), however, the cytosol is the target site for delivery; hence, passage across the nuclear membrane is not needed.

To achieve a high level of transfection after successful delivery of a gene, many factors need to be taken into consideration. These include—but are not limited to—carrier types and their morphology, molecular weight, negative to positive (N/P) charge ratios between gene and carrier, particle size, ζ -potential, salt concentration, the type/size of the gene, and the cell line to which delivery is required. However, despite all of the data published to date in this area, rational design principles for cationic vectors to optimize the efficiency of transfection are still lacking. The parameters mentioned above that have been reported vary considerably from study to study, with many discrepancies and contradictions apparent in experimental models. To highlight this, Table 1 summarizes the structure/function relationships of various polyplexes in gene delivery.^{8–20} In biological experiments, the strength of DNA compaction is commonly measured by the ethidium bromide titration assay.^{8,9} When the polycation carrier binds to a gene, it leads to the exclusion of ethidium bromide dye from the gene structure and a net decrease in fluorescence. A relatively tight binding affinity between cation and gene is indicated by a net lowering of fluorescence. Mann et al. compared the interactions of DNA with poly(L-lysine) (PLL) of various lengths (average 19, 41, and 120 residues) at different DNA concentrations (3–20 ng/ μ L).²¹ The results indicated that PLL of the smallest length chosen was the most efficient in condensing DNA at low DNA concentrations. On the contrary, Shen et al. studied the formation of RNA/poly(amidoamine) (PAMAM) dendrimers using atomic force microscopy.²² They found that higher generations of dendrimers can form stable and uniform RNA/dendrimer complexes. It is possible that molecular heterogeneities among

* To whom correspondence should be addressed. (H.S.P.) Tel: +61-7-3365 7430. Fax: +61-7-3365 1688. E-mail: h.parekh@pharmacy.uq.edu.au. (S.C.S.) Tel: +61-7-3346 3949. Fax: +61-7-3346-3992. E-mail: s.smith@uq.edu.au.

[†] School of Pharmacy, The University of Queensland.

[‡] Australian Institute of Bioengineering and Nanotechnology, The University of Queensland.

[§] Universität Heidelberg.

TABLE 1: Different Behaviors of Branched and Linear Carriers for Gene Delivery In Vitro or In Vivo

	carriers	gene	cell lines or animal models	results
PLL	linear PLL 2.9 kDa; linear PLL 20 kDa; dendritic PLL G3 (eight primary amines); dendritic PLL G5 (32 primary amines)	β -galactosidase and luciferase encoding plasmids with cytomegalovirus promoter ($P_{CMV}\beta$)	retinal pigment epithelial cells (D407)	Linear PLL was better than dendritic shape for cell uptake and transfection efficiency in vitro
	linear PLL 20 kDa; linear PLL 211 kDa	6.4 kb pDNA	female Balb/c mice and Wistar rats	The PLL20/DNA complex is more easily cleared in vivo. ⁸⁴
	dendritic G6 PLL (KG6) (128 amines); linear PLL (170 amines)	pDNA (PGV-C/CMV)	CHO cells	More weakly compacted DNA with KG6 and higher transfection efficiency was than that of linear PLL. ⁸
polyethylenimine (PEI)	linear PEI 22 kDa; branched PEI 25 kDa	plasmid pSV- β -gal	murine B16F10 melanoma cells; murine MCA-38 colon carcinoma cells; murine C-26 colon carcinoma cells	Linear PEI is better than branched PEI in vitro. ¹⁵
	linear PEI 22 kDa; branched PEI 25 kDa	SMD2-Luc Δ ITR (7.6 kb)	HepG2 cells and female Balb/c mice	Linear PEI is better than branched PEI in vivo. ¹⁴
	branched PEI 5.4 kDa; branched PEI 25 kDa	pDNA	L929, NIH-3T3, 293, COS-K1, Hela, and Jurkat cell lines; Balb/c mice	Linear PEI shows a higher transfection efficiency and lower toxicity than H-PEI. ¹²
	linear PEI 1–9.5 kDa; linear PEI 22 kDa	pDNA	CHO-K1 and HeLa cells	Linear PEI with low MWs are more efficient and less toxic than high MW linear PEI.
DNA	branched PEI 10, 25, and 70 kDa; linear PEI 25 kDa	pCMV-Luc	female ICR mice	Linear PEI is better than branched PEI. ¹³
	branched PEI 2, 25, and 750 kDa; linear PEI 25 kDa;	plasmid pSP-E1A, pEAK8-EGFP and RNA	no cell experiments	Branched PEIs have a higher affinity for DNA than linear PEIs. ¹⁰
PAA	branched PEI 25 kDa; branched PLL 25 kDa; Lipofectamine2000	circular pDNA (c-DNA), linear pDNA (l-DNA)	rat bone marrow stromal cells	Gene delivery is mainly determined by the nature of gene carriers, and circular DNA was more effective than linear DNA. ¹⁸
	branched and linear poly(glycoamidoamine)	pDNA	HeLa cells	In general, linear structures had higher transfection efficiency and toxicity than branched analogues. ¹⁷

the polyplexes that are formed might be a potential reason for the apparently contradicting conclusions derived in different experimental reports. The dependence of polyplex structures on sometimes minute variations in experimental conditions has recently been studied by use of techniques from single-molecule fluorescence spectroscopy and fluorescence fluctuation spectroscopy, opening the agenda of more detailed studies of molecular interaction in polyplexes.^{23–25}

Given the discussion above, our focus has been drawn toward gaining a better understanding of and ultimately quantifying the underlying factors that influence the binding of carrier and gene—an issue that has been largely overlooked to date when designing nonviral vectors. Control of the strength of such binding is expected, however, to be an important factor in achieving release of the gene once at the target site. Direct experimental studies of gene–carrier complexation are very sparse due to the experimental difficulties. However, molecular dynamics (MD) simulations offer considerable potential to shed light on this phenomenon, as illustrated in the present study.

To date, only a handful of theoretical studies describing gene–polycation complexation have been reported.^{26–32} Lyulin et al. performed extensive coarse-grained MD simulations to study the complex formed between cationic dendrimers and negatively charged linear polyelectrolytes.²⁷ It was reported that the complexation of a linear polyelectrolyte with a dendrimer results in an obvious compaction of the complex and dehydration of the chain. In addition, counterions locating on or within the structure of the dendrimer–polyelectrolyte complex were found

to enhance the strength of existing electrostatic interactions. In another theoretical study, cationic lipid–DNA complexes have been investigated using a coarse-grained molecular model alongside Monte Carlo simulations.^{28,29} This is a self-assembly system comprised of a cationic liposome–DNA complex. The DNA–interaxial spacing has a linear relationship with the fraction of charged lipids, which is confirmed by experimental X-ray diffraction. The data demonstrated that an increase in charge density of the liposome–DNA complex membrane leads to a decrease in the mechanical stability of the complex. This invoked an explanation for the improved transfection efficiency of lamellar cationic lipid–DNA complexes with high charge density. Nikakhtar et al. also built one mathematical model for the formation and stability prediction of DNA–dendrimer nanoclusters.³³ This model assumed that the DNA molecule was an inextensible semiflexible polymer model (or wormlike chain model) and applied the nonlinear Poisson–Boltzmann equation. The free energy of this model is the combination of electrostatic contribution between DNA and cationic polymer and elastic contribution of DNA chain wrapped around the polymer.

The aforementioned research provides us with some structural details of dendrimer–polyelectrolyte complexes; however, when using the simple bead models of dendrimers and nucleic acids, the precision of the model is limited. In 1999, Bandyopadhyay et al. studied lipid–DNA interactions by MD simulation and found that both cationic lipids (dimyristoyltrimethylammonium propane, DMTAP) and amphiphilic lipid (dimyristoylphosphatidylcholine, DMPC) interacted with the anionic DNA phosphate

TABLE 2: Simulation Cell Compositions and Atom Numbers for the Systems of Cationic Polymers–siRNA Complexation

	4 ⁺ dendron–RNA complex		4 ⁺ G0–RNA complex		4 ⁺ linearlysine–RNA complex		8 ⁺ dendron–RNA complex		8 ⁺ G1–RNA complex		8 ⁺ linearlysine–RNA complex	
	major groove	minor groove	major groove	minor groove	major groove	minor groove	major groove	minor groove	major groove	minor groove	major groove	minor groove
atom number of RNA	1335	1335	1335	1335	1335	1335	1335	1335	1335	1335	1335	1335
atom number of polymers	78	78	88	88	104	104	166	166	236	236	192	192
number of Na ⁺	36	36	36	36	36	36	32	32	32	32	32	32
molecule number of water	8712	8796	8764	8694	8889	8809	8852	8663	9025	8805	8816	9093
total atom number	27585	27837	27751	27541	28142	27902	28089	27522	28678	28018	28007	28838

groups.³⁴ Recently, Thyveetil et al. performed large-scale MD simulations to investigate the structural stability and material properties of DNA-intercalated layered double hydroxides (LDHs).^{30,31} They found that a strong electrostatic interaction between LDH sheets and intercalated DNA restricted the movement of DNA molecules in this system, which led to the enhanced structural stability of DNA when compared to DNA alone in aqueous solution. In recent years, there has only been one report describing the full atomistic MD simulation of dendrimer–DNA complexes.³² Maiti et al. studied the structure and dynamics of single-strand DNA–PAMAM dendrimer complexation in explicit water and counterions by atomistic MD simulations.³² The results indicated that the complexation between positively charged dendrimers and the negatively charged DNA molecule is a free energy minimum process and shows strong sequence dependence. Different protonation levels of the generation 2 to 4 (G2 to G4) PAMAM–DNA complex in explicit water and counterions were discussed in detail. Experimental results have revealed that single-stranded DNA–PLL complexes are much smaller and more stable in physiological salt (NaCl) solutions than that of double-stranded DNA;³⁵ hence, there is clearly a considerable difference between single-stranded and double-stranded DNA in this context. More recently, modeling and multivalent recognition between dendritic molecules with spermine surface groups and DNA were studied by MD methods.³⁶ Energetic effects, ligand sacrifice effects, and binding sites were studied in detail.

In this study, we explore via atomistic MD simulations the complexation between a 21 base pair duplex small interfering RNA (siRNA) and six cationic polymers of varying structure in explicit water and counterions. Specifically, we studied a four positive-charged G0-PAMAM dendrimer (4⁺dendrimer); an eight positive-charged G1-PAMAM dendrimer (8⁺dendrimer); a four positive-charged dendritic PLL (4⁺dendron); an eight positive-charged dendritic PLL (8⁺dendron); a four positive-charged linear PLL (4⁺linearlysine); and an eight positive-charged linear PLL (8⁺linearlysine) (as shown in Figure S-1 in the Supporting Information). Binding free energies of their complexation are estimated by the MM-PBSA method^{37–42} in AMBER9^{43–45} and are discussed in relation to structure and dynamical properties of the siRNA and their carriers. In section 2 below, we summarize the details of MD simulations and MM-PBSA calculations, and section 3 provides results and discusses the relationships that we discovered between charges and binding free energies in gene release, followed by concluding remarks in section 4.

2. Simulation Details

2.1. MD Simulations. The sequence of the 21 base pair siRNA is taken from the earlier study by Putral et al.⁴⁶ and is as follows:

sense: 5'-GCAACAGUUACUGCGACGUUU-3'

antisense: 3'-UUCGUUGUCAAUGACCGCUGCA-5'

The MD simulations utilize the AMBER9 software package^{43–45} with the all-atom ff99 force field for RNA⁴⁷ and the general AMBER force field (gaff) for all polymers.⁴⁸ Duplex RNA was generated by the Nucleic Acid Builder (NAB) (<http://casegroup.rutgers.edu/>). All six different polymers were built by Material Studio 4.3 (<http://accelrys.com/products/materials-studio/>), and all of the primary amines were protonated. Using the LEAP module in AMBER 9, the polymer was positioned in the major groove or minor groove of RNA. The electrostatic interactions were calculated with the particle mesh Ewald method,^{49–54} and the cutoff was 10 Å. Using the LEAP module in AMBER 9, the complex structure was immersed in a truncated octahedral water box with a solvation shell of 8 Å thickness using the TIP3P model for water.⁵⁵ In addition, some water molecules were replaced by Na⁺ counterions to neutralize the negative charge on the phosphate backbone of the RNA structure. This procedure resulted in solvated water structures containing approximately 30000 atoms, which included the 1335 RNA atoms and either 32 or 36 counterions (Na⁺), with the remainder being water molecules. The composition of these systems is shown in Table 2.

The minimization procedure for solvated RNA consisted of two steps. In the first, the complex was kept fixed, and positions of the water and ions were minimized. The solvated structures were then subjected to 1000 steps of steepest descent minimization followed by 1000 steps of conjugate gradient minimization.^{56,57} During this minimization process, the complex was kept fixed in its starting conformation using harmonic constraints with a force constant of 500 kcal/mol/Å². In the second stage, the entire system was minimized by 2000 steps of steepest descent minimization followed by 8000 steps of conjugate gradient minimization without the restraints.

The minimized structure was then subjected to 20 ps of MD, using a 2 fs time step for integration. During the MD simulation, the system was gradually heated from 0 to 300 K using 10 kcal/mol/Å² weak positional restraints on the RNA. The SHAKE algorithm was used in which all bonds involving hydrogen are constrained.⁵⁸ After the system was heated at a constant volume with weak restraints on the complex, MD was performed for 18 ns with a time step of 2 fs under constant pressure/constant temperature (NPT ensemble) at 300 K with an average pressure of 1 atm without positional restraints. The random number seed of every restart was changed.⁵⁹ Isotropic position scaling⁶⁰ was used to maintain the pressure, and a relaxation time of 2 ps was employed. SHAKE was used to constrain bonds involving hydrogen, and the temperature was kept at 300 K with Langevin dynamics⁶¹ using a collision frequency of 1.0 ps⁻¹.

2.2. MM-PBSA Free Energy Calculations. The binding free energy for each complex was calculated using the MM-PBSA method in AMBER9.^{37–42} In this method, the average interaction energies of the receptor and the ligand were calculated using an ensemble of snapshot structures taken from the MD trajectory of the system. The binding free energy in

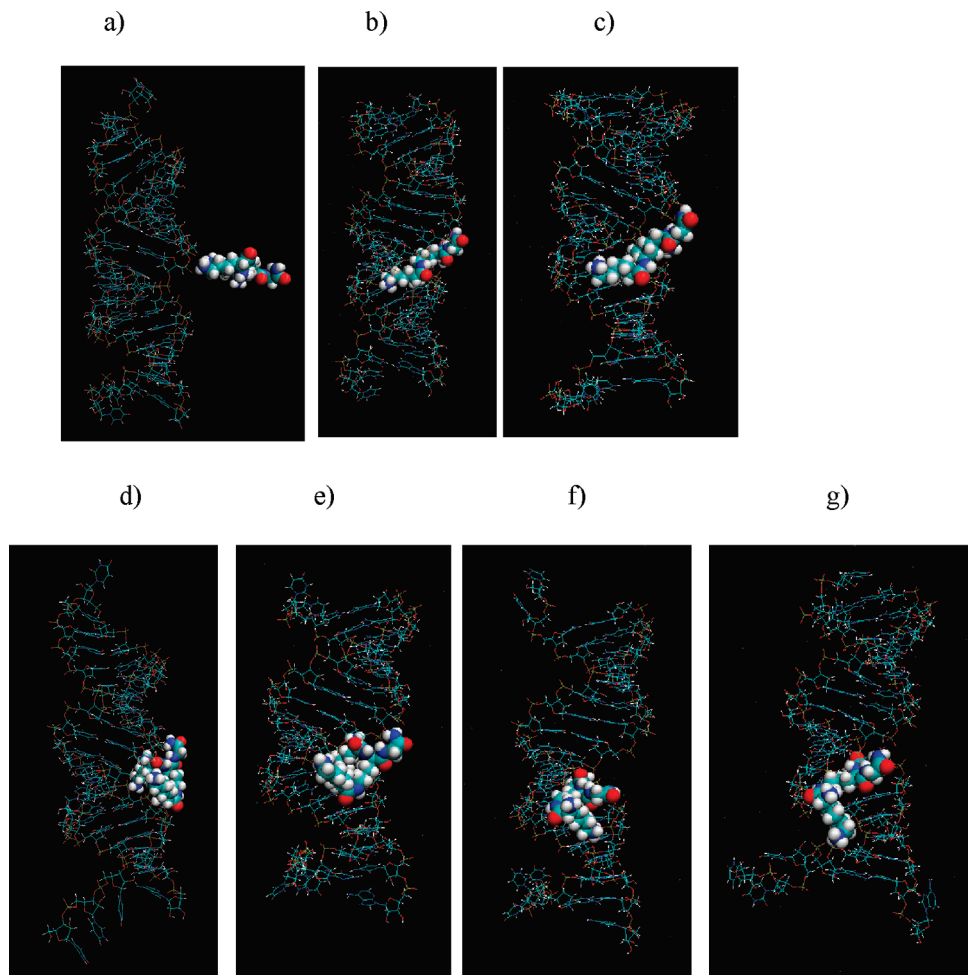


Figure 1. Snapshots of the 4^+ dendron complexed with RNA when the starting position is adjacent to the major groove: (a) at 0 ns, (b) after 3 ns, (c) after 6 ns, (d) after 9 ns, (e) after 12 ns, (f) after 15 ns, and (g) after 18 ns.

solution (ΔG_{bind}) was computed from the solvation free energies for the receptor, the ligand, and the complex [$\Delta G_{\text{water}}(\text{receptor})$, $\Delta G_{\text{water}}(\text{ligand})$, and $\Delta G_{\text{water}}(\text{complex})$]:

$$\Delta G_{\text{bind}} = \Delta G_{\text{water}}(\text{complex}) - [\Delta G_{\text{water}}(\text{receptor}) + \Delta G_{\text{water}}(\text{ligand})] \quad (1)$$

The free energies for each species (the receptor, the ligand, and the complex), ΔG_{water} , were calculated using the following equations:

$$\Delta G_{\text{water}} = E_{\text{MM}} + G_{\text{solvation}} - TS \quad (2)$$

$$G_{\text{solvation}} = G_{\text{PB}} + G_{\text{nonpolar}} \quad (3)$$

$$E_{\text{MM}} = E_{\text{internal}} + E_{\text{electrostatic}} + E_{\text{vdW}} \quad (4)$$

$$E_{\text{internal}} = E_{\text{bond}} + E_{\text{angle}} + E_{\text{torsion}} \quad (5)$$

where E_{MM} is the absolute molecular mechanical energy; $G_{\text{solvation}}$ is the solvation free energy; G_{PB} is the electrostatic solvation free energy; G_{nonpolar} is the nonpolar solvation free energy;

$E_{\text{electrostatic}}$ and E_{vdW} are the electrostatic and van der Waals interaction energies, respectively; the internal energy E_{internal} is determined by E_{bond} , E_{angle} , and E_{torsion} , which represent the strain energy in bonds, angles, and torsion angles; T is the temperature; and S is the entropy.

The entropy contributions were determined by the NMODE program within AMBER, but in practice, these values are ignored because different polymers to the same nucleic acid show similar entropy for a comparison of states and their calculations need quite costly computing abilities. The E_{MM} value of each snapshot was calculated using the ANAL program of AMBER with all pairwise interactions included using a dielectric constant (ϵ) of 1. The E_{internal} value always amounts to zero in the single trajectory approach. The solvation free energy ($G_{\text{solvation}}$) was estimated by two different approaches: the Poisson–Boltzmann finite-difference equation (FDPB)^{62–64} and the generalized Born approach (GB).^{65–70}

We used $\epsilon = 1$ for the solute and $\epsilon = 80$ for the solvent in the electrostatic solvation free energy ($-G_{\text{PB}}$) calculations. A solvent probe radius of 1.4 Å was used to the molecular surface.⁷¹ Atomic charges of the Cornell et al. force field were used for calculating the total electrostatic energies.⁷² An 80% boxfill cubic lattice and a grid resolution of 0.5 Å/grid point were used in the PB calculations. The nonpolar contribution to the solvation free energy was determined with solvent-acces-

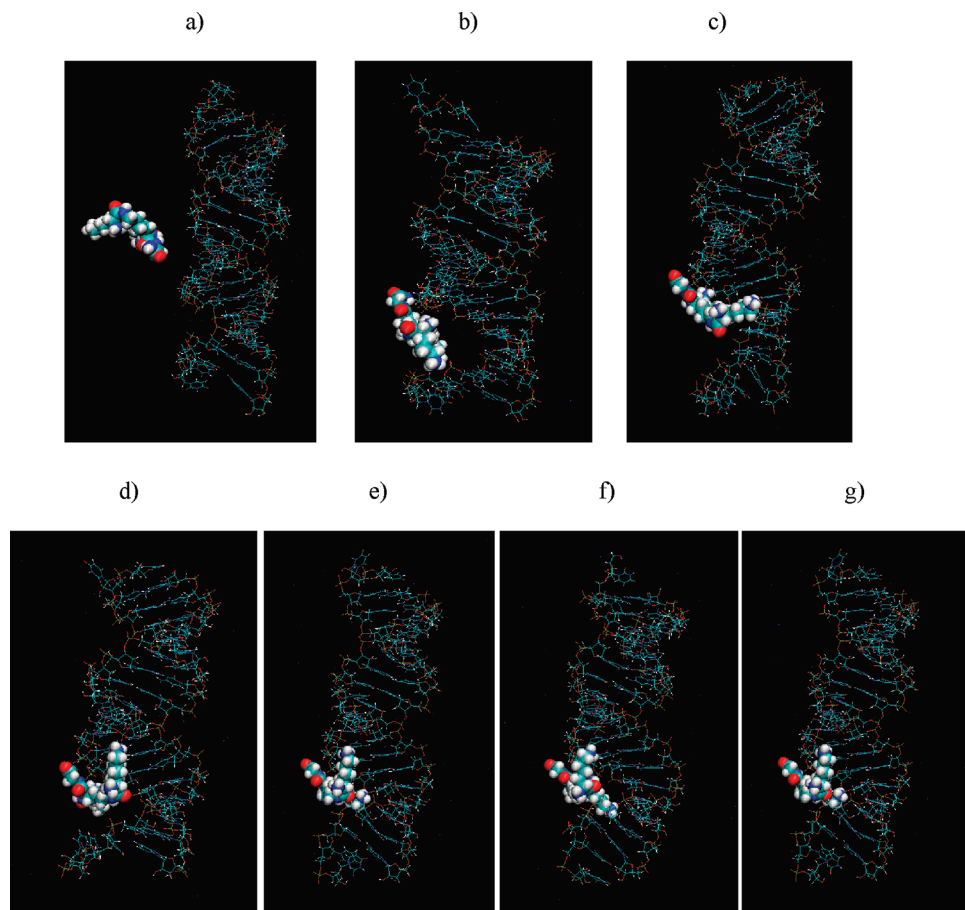


Figure 2. Snapshots of the 4^+ dendron complexed with RNA when the starting position is adjacent to the minor groove: (a) at 0 ns, (b) after 3 ns, (c) after 6 ns, (d) after 9 ns, (e) after 12 ns, (f) after 15 ns, and (g) after 18 ns.

sible-surface-area (SASA) terms with the *molsurf* program.^{73,74} The *molsurf* program was used to calculate the nonpolar solvation free energy (G_{nonpolar}) as follows:

$$G_{\text{nonpolar}} = \text{SURFTEN} \times \text{SASA} + \text{SURFOFF} \quad (6)$$

where SURFTEN is 0.0072 kcal/ \AA and SURFOFF is 0 kcal/mol.⁷¹

Binding free energy calculations were performed using single polymer–RNA trajectories. This meant that the snapshot structures for the energy calculations of the polymer–RNA complex and separated polymer and RNA were taken from the unbound polymers, unbound RNA, and the complexes. From the last 2 ns of each equilibrated trajectory in 10 ps intervals, 200 snapshots were taken at even intervals for the binding energy analyses, and the reported binding free energies are averages of the 200 snapshots.

3. Results and Discussions

3.1. Structural Aspects of the Complex. Snapshots at 3 ns intervals during the 18 ns MD simulations are shown for the PLL 4^+ dendron in Figures 1 and 2. Figure 1 is derived from a simulation in which the 4^+ dendron was initially positioned near the major groove at the middle of the strand, while Figure 2 relates to a simulation where the dendron was positioned near the minor groove at the middle of the strand. Analogous results for the PAMAM 4^+ G1 and 4^+ linearlysine are shown in Figure S-2 (see the Supporting Information). From these figures, a very interesting result becomes apparent: The 4^+ polymers all bind

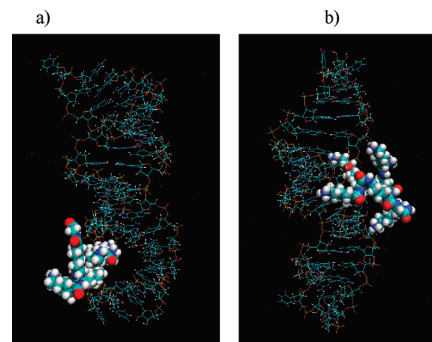


Figure 3. Snapshots of 8^+ dendron complexed with RNA after 18 ns of simulation (a) when the starting position was adjacent to the minor groove of RNA and b) when the starting positions was adjacent to the major groove of RNA.

on the major groove of the siRNA, even if they were placed initially on the minor groove side of the nucleic acid. During MD simulations, it is evident that the carriers gradually change their position from the minor groove to the major groove. However, as Figure 3 and Figure S-3 in the Supporting Information show, the 8^+ polymers show less specific regional binding on the gene, with binding seen on both the major groove and the minor groove. This finding is in accordance with previous reports and can be attributed to differences in averaged hydration diameters of our 4^+ and 8^+ polymers, which are found to be about 11 ($\sim 5.5 \text{ \AA}$ for averaged radius of gyration) and 16.4 \AA ($\sim 8.2 \text{ \AA}$ for averaged radius of gyration), respectively.³² Being larger than the width of the major groove, our 8^+ polymers are unable to be accommodated within RNA helices, and so,

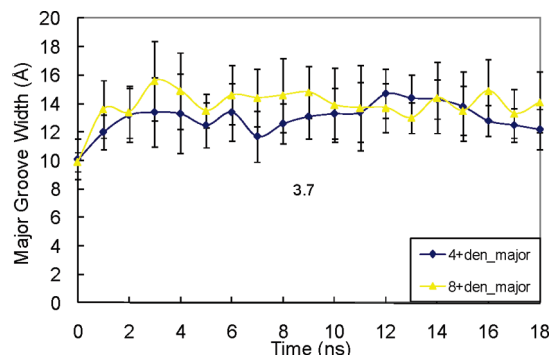


Figure 4. Major groove width of siRNA (averaged along the strand) vs time for 4+dendron– or 8+dendron–RNA complexation during 18 ns simulations. The major groove width is defined as averaged direct P–P distances of base pairs. The error bars indicate the standard deviation associated with averaging along the length of the strand.

preferential binding was not observed. One may plausibly infer that the factors governing whether a molecule can fit in the major groove or minor groove is dependent upon its molecular volume as well as the width of major groove of the nucleic acid. If the carrier is too large to be accommodated in the major groove, it will bind in a less specific manner across minor and major grooves. In the same time frame, as Figure 4 demonstrates, there is a fluctuation of the major groove width of RNA in the complexation, which is in accordance with our previous simulations of siRNA.⁷⁵ The major groove width was calculated with the 3DNA software⁷⁶ and is seen to fluctuate typically between 10 and 16 Å during the simulations. Shown in Figure 4 is the variation in the major groove width (averaged along the strand) as a function of simulation time for the PLL 4⁺dendron and 8⁺dendron complexes. The bars indicate the standard deviation associated with averaging along the length of the strand at any given time.

It is apparent from the snapshots of Figures 1–3 and structural parameters of siRNA in Table 3 that there are strong duplex–RNA deforming characteristics in the presence of polymer, with the terminal amine group of polymer also making contact with the phosphate groups of the RNA. Despite this, one may observe that the cationic charge density of even our 8⁺polymer is not strong enough to enable the RNA molecule to fully wrap around the polymer; as a result, there were some positive charges of the dendrimers that did not make contact with all negatively charged phosphate groups on RNA.

3.2. Dynamics of the Complex Formation. The root-mean-squared deviation (rmsd) plots for the polymer–RNA complexes

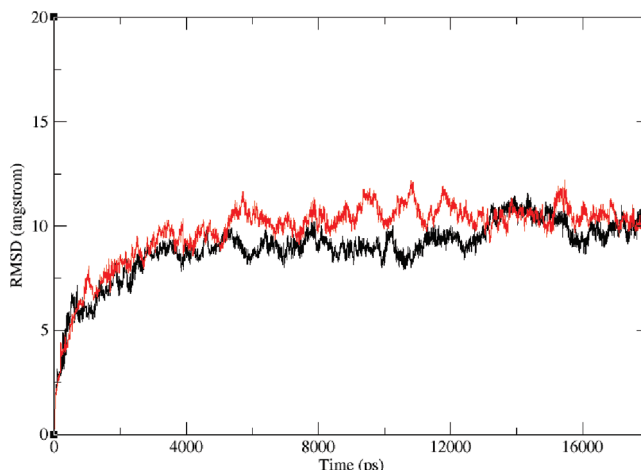


Figure 5. rmsd vs time for 4+dendron– and 8+dendron–RNA complexation over the 18 ns simulations, shown for the cases where the dendrons start out adjacent to the major groove (see, for example, Figure 1). The rmsd is mass weighted for polymer–RNA complexes, with water and counterions not included. Black line, 4+dendron complex; and red line, 8+dendron complex.

are shown in Figure 5 and represent the fluctuation of the atoms on the backbone of the complex. It is quite obvious that this parameter is relatively stable after 5 ns, which is indicative that our complexes are reasonably equilibrated during the time scale of our 18 ns simulations. During the MD simulations, as implied by the snapshots of Figures 1 and 2, the carriers gradually change their position and then merge with the gene. This process can be tracked by examining the numbers of close contacts between carrier and gene as the simulation proceeds. In Figure 6, the time dependence of the number of contacts between RNA and polymer is shown for the four simulations represented in Figures 1 and 2. It is apparent that the number of contacts rises sharply during the first ns of the simulation. For the smaller 4⁺dendron, the number of contacts has already stabilized at 1 ns, whereas for the larger 8⁺dendron, the number continues to increase gradually until it stabilizes around 8 ns. It is also obvious that a greater number of contacts is achieved for the larger dendron, as would be expected. Overall, this behavior reflects a process of quick binding of RNA with the cation followed by minor adjustments to their configuration as final equilibration is reached.

In general, water and counterions play an important role in the complexation between polymer and nucleic acid with the entropy loss and enthalpy gain. Insights into this process can

TABLE 3: Starting Structures and Average Structures of siRNA in the 18 ns Simulation for the Backbone Angles and Helical Parameters

	starting structures	4 ⁺ dendron major	4 ⁺ dendron minor	8 ⁺ dendron major	8 ⁺ dendron minor
x-disp (Å)	-4.61 ± 0.28	-4.57 ± 0.86	-4.33 ± 0.97	-4.44 ± 0.97	-4.38 ± 0.75
y-disp (Å)	-0.01 ± 0.05	-0.05 ± 0.42	-0.07 ± 0.86	-0.14 ± 0.82	0.08 ± 0.90
inclination (°)	16.02 ± 0.68	16.89 ± 7.96	17.29 ± 7.44	16.55 ± 9.13	16.77 ± 8.12
shift (Å)	0.00 ± 0.02	0.03 ± 0.18	0.00 ± 0.20	-0.06 ± 0.44	0.01 ± 0.22
slide (Å)	-1.75 ± 0.03	-1.60 ± 0.13	-1.42 ± 0.38	-1.44 ± 0.70	-1.46 ± 0.44
rise (Å)	3.40 ± 0.01	3.31 ± 0.16	3.31 ± 0.22	3.36 ± 0.27	3.34 ± 0.29
tilt (°)	0.00 ± 0.08	0.11 ± 1.05	0.21 ± 2.40	0.15 ± 1.22	0.68 ± 3.12
roll (°)	8.91 ± 0.12	8.91 ± 4.16	9.10 ± 4.13	8.52 ± 4.80	8.96 ± 4.52
twist (°)	31.55 ± 1.23	29.68 ± 1.78	29.34 ± 2.74	28.83 ± 2.18	29.26 ± 2.10
shear (Å)	0.00 ± 0.11	0.14 ± 0.60	-0.08 ± 0.39	0.09 ± 0.48	0.07 ± 0.31
stretch (Å)	-0.12 ± 0.06	-0.14 ± 0.10	-0.33 ± 0.24	-0.26 ± 0.57	-0.17 ± 0.13
stagger (Å)	0.03 ± 0.00	-0.13 ± 0.48	0.09 ± 0.29	-0.14 ± 0.26	-0.15 ± 0.49
buckle (°)	0.00 ± 0.20	-0.74 ± 4.72	0.16 ± 5.35	0.62 ± 8.15	0.56 ± 7.20
propol (°)	13.74 ± 0.01	-16.37 ± 8.35	-13.50 ± 3.95	-11.89 ± 4.53	-13.14 ± 3.61
opening (°)	-5.52 ± 0.13	0.15 ± 4.89	-0.92 ± 1.32	0.66 ± 2.59	0.96 ± 2.03

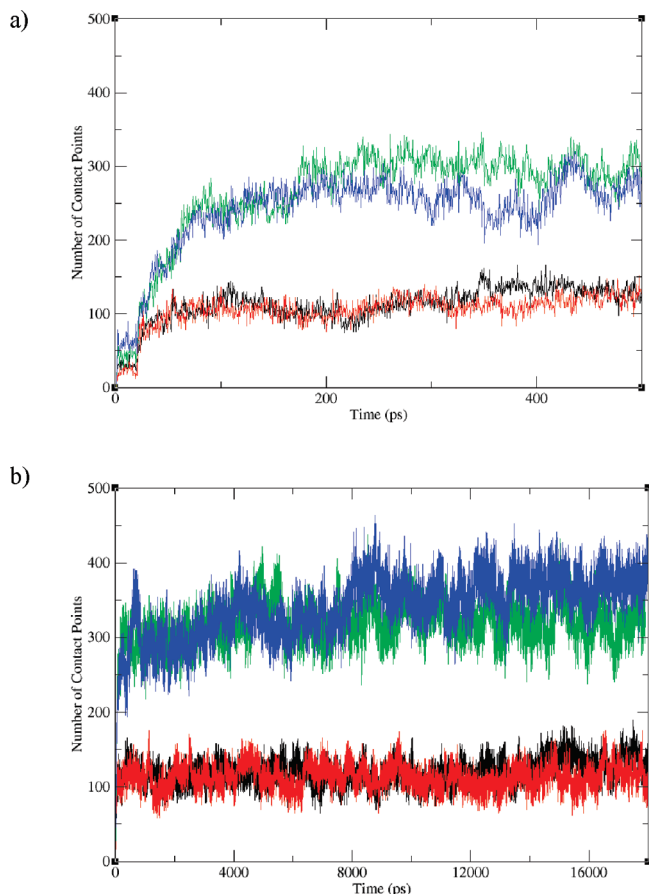


Figure 6. Variation of the number of contact points between PLL dendrons and RNA (any contact within 3 Å) during the 18 ns simulations. Panel a shows early time behavior during the first 500 ps, while panel b shows the behavior over the whole 18 ns. The black line (lower curve dark) is the 4+dendron complexed with RNA with the starting position adjacent to the major groove. The red line (lower curve light) is the 4+dendron complexed with RNA with the starting position adjacent to the minor groove. The blue line (upper curve dark) is 8+dendron complexed with RNA with the starting position adjacent to the major groove. The green line (upper curve light) is the 8+dendron complexed with RNA with the starting position adjacent to the minor groove.

be gleaned by examining the number of hydrating water molecules around the dendrimer as a function of time during the complexation process. Figure 7 shows the plot of the number of water molecules that are within 3 Å of the PLL dendrons versus time. It is obvious that the number of solvating water molecules decreases significantly during the complexation process. In general, this phenomenon may be rationalized in terms of two factors: (i) structural compaction effects induced by the complexation, which decrease the available volume within the system for the solvating water molecules, and (ii) effective displacement of hydrating water molecules by the other partner in the complex (in this case the siRNA). Given that the present study involves relatively small dendritic carriers, we anticipate that structural compaction is less likely to be a major factor and hence conclude that the reduction in numbers of solvating water molecules shown in Figure 7 is better interpreted as effective displacement of water around the dendrimer by the RNA complex partner. This said, it should also be pointed out that the effective equilibration of the solvating waters in the system is apparently a more subtle dynamical process that occurs on a longer time scale than other processes that we have examined above. For example, the number of contacts between

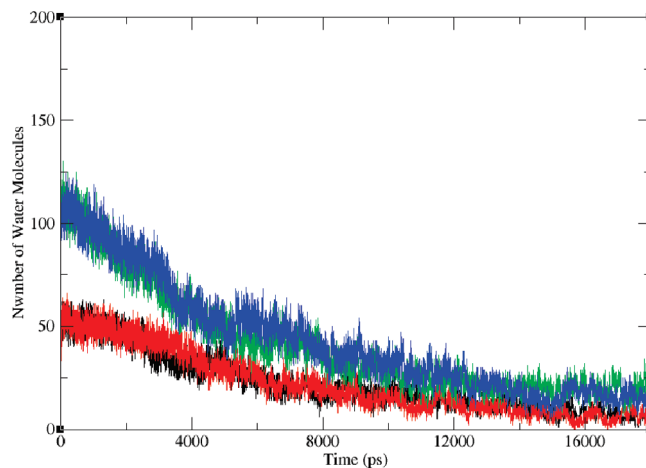


Figure 7. Number of water molecules in a spine of hydration (any contact within 3 Å of the polymer) as a function of time for complexation between PLL dendrons and RNA during the 18 ns simulations. Line definitions are the same as for Figure 6.

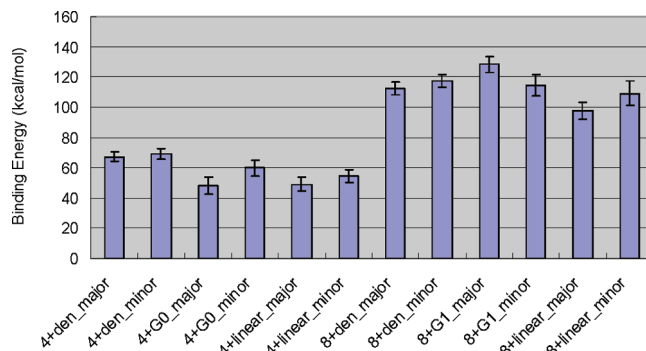


Figure 8. Dissociation free energies for the polymer–RNA complex in the minor or major groove.

dendron and RNA (Figure 6) stabilizes within the first 500 ps for the smaller 4+dendron and over the first 8 ns for the 8+dendron, while the rmsd has stabilized after approximately the first 6 ns (Figure 5). On the other hand, the number of hydrating water molecules is still adjusting significantly in Figure 7 out to about 16 ns. The general behavior observed in Figure 7 correlates qualitatively with experimental observations provided by the ethidium bromide titration assay.^{8,9}

3.3. Binding Free Energies and Dissociation Free Energies. We have estimated binding free energies for the range of carrier systems investigated using the methods summarized in section 2, and the results are presented in Table 4. As compared to other free energy methods, such as thermal integration and umbrella sampling, the MM-PBSA method is both cost-effective and of sufficient accuracy for the present exploratory purposes. It is widely used for the evaluation of binding affinities between ligands and receptors, one of the most important challenges in theoretical drug design.^{37–42} From the values in Table 4, it is clear that electrostatic interactions play a primary role in the association of gene and dendron. For example, a value of 39.54/67.17 kcal/mol (or 59%) can be attributed to the electrostatic affinity of 4+dendron–RNA complex in the major groove. van der Waals forces were found to be the second highest contributor responsible in gene–dendron binding, which was 22.23/67.17 kcal/mol (or 33%) for the 4+dendron–RNA complex in the major groove. The lowest contributing factor to complexation was nonpolar solvation terms, comprising 5.40 kcal/mol (or 8%) for the 4+dendron–RNA complex in the major groove. These values confirm previous predictions that polycation–DNA or

TABLE 4: Binding Free Energies for the Polymer–RNA Complex in the Minor or Major Groove Using the MM-PBSA Method^a

	4 ⁺ dendron–RNA complex						4 ⁺ linearlysine–RNA complex						8 ⁺ dendron–RNA complex						8 ⁺ linearlysine–RNA complex						
	major groove			minor groove			major groove			minor groove			major groove			minor groove			major groove			minor groove			
	major groove	minor groove	major groove	minor groove	major groove	minor groove	major groove	minor groove	major groove	minor groove	major groove	minor groove	major groove	minor groove	major groove	minor groove	major groove	minor groove	major groove	minor groove	major groove	minor groove	major groove	minor groove	major groove
ΔE_{elec} (kcal/mol)	-3516.97 (25.63)	-3312.47 (24.79)	-3273.51 (67.44)	-3020.98 (78.06)	-2899.25 (36.50)	-2843.41 (39.53)	-6540.00 (89.92)	-5647.10 (44.39)	-5742.27 (52.80)	-5771.37 (58.76)	-6358.45 (49.07)	-5717.58 (40.83)													
ΔE_{vdW} (kcal/mol)	-22.23 (3.61)	-24.85 (3.57)	-18.06 (3.77)	-18.00 (4.43)	-21.69 (3.00)	-26.70 (3.42)	-23.56 (4.57)	-31.18 (4.84)	-49.57 (4.05)	-51.87 (4.41)	-19.85 (3.94)	-28.84 (4.89)													
ΔE_{MM} (kcal/mol)	-3539.19 (25.88)	-3337.33 (24.78)	-3291.58 (69.11)	-3038.98 (81.10)	-3120.93 (36.60)	-2870.11 (39.68)	-6563.56 (90.71)	-5678.28 (44.37)	-5791.84 (52.17)	-5823.24 (59.27)	-6378.30 (49.03)	-5746.42 (40.18)													
$\Delta \Delta G_{\text{bp}}$ (kcal/mol)	-5.40 (0.18)	-6.40 (0.22)	-5.03 (0.43)	-4.83 (0.73)	-4.94 (0.32)	-6.18 (0.22)	-7.96 (0.33)	-7.56 (0.20)	-9.72 (0.33)	-10.54 (0.20)	-7.92 (0.30)	-6.63 (0.16)													
$\Delta \Delta G_{\text{PB}}$ (kcal/mol)	3477.42 (25.12)	3274.70 (24.30)	3248.38 (64.72)	2983.87 (78.55)	3076.66 (34.36)	2821.75 (37.42)	6458.98 (89.33)	5568.45 (43.32)	5673.26 (51.27)	5719.02 (58.64)	6288.43 (45.98)	5643.86 (38.76)													
$\Delta \Delta G_{\text{solv}}$ (kcal/mol)	3472.03 (25.01)	3268.30 (24.30)	3243.35 (64.33)	2979.05 (77.89)	3071.72 (34.19)	2815.57 (37.31)	6451.02 (89.11)	5560.90 (43.25)	5663.54 (51.14)	5708.49 (58.57)	6280.51 (45.78)	5637.23 (38.70)													
$\Delta \Delta G_{\text{elec}}$ (kcal/mol)	-39.54 (4.54)	-37.77 (4.97)	-25.14 (5.36)	-37.11 (4.61)	-22.58 (4.53)	-21.66 (5.52)	-81.03 (6.79)	-78.65 (6.73)	-69.02 (6.52)	-52.34 (9.07)	-70.02 (7.02)	-73.73 (11.51)													
ΔG_{bind} (kcal/mol)	-67.17 (3.12)	-69.03 (3.40)	-48.23 (5.84)	-59.94 (5.13)	-49.21 (4.27)	-54.53 (4.32)	-112.54 (4.29)	-117.39 (4.30)	-128.30 (5.11)	-114.75 (6.95)	-97.79 (5.51)	-109.20 (8.05)													
$\Delta G_{\text{dissociation}}$ (kcal/mol)	67.17	69.03	48.23	59.94	49.21	54.53	112.54	117.39	128.30	114.75	97.79	109.20													

^a Note the following: (1) The major (or minor) groove refers to the starting structure of the complex, not the final structure. (2) Average over 200 snapshots from the last 2 ns trajectory; the standard error of the mean is in parentheses. (3) Definition of energy contributions: ΔE_{elec} , electrostatic molecular mechanical energy; ΔE_{vdW} , van der Waals molecular mechanical energy; $\Delta E_{\text{elec}} = \Delta E_{\text{elec}} + \Delta \Delta G_{\text{bp}}$; $\Delta \Delta G_{\text{bind}} = \Delta \Delta G_{\text{bp}} + \Delta \Delta G_{\text{solv}}$; and ΔG_{bind} , calculated binding energy.

RNA complexation depends primarily on electrostatic interactions between the positive-charged carrier and the negative-charged phosphate groups on the backbone of nucleic acids.^{1,2}

One exception to the overall trend summarized above is in the case of 4⁺linearlysine–RNA complexation in the minor groove, in which the contribution of van der Waals (26.70 kcal/mol) is greater than that of the electrostatic interaction (21.66 kcal/mol). The most likely reason for this is that the linear polymer in question is constrained by a very short amide backbone, rendering it less flexible and so less amenable to folding necessary for complementary binding by charge–charge interactions. Furthermore, this short, rigid backbone along with the alkyl portion of the lysine side chain form a significant proportion of the entire 4⁺polymer, which is ultimately responsible for hydrophobic interaction with RNA. This is further corroborated by 4⁺linearlysine–RNA complex binding in the more accessible major groove, in which the contribution of van der Waals (21.69 kcal/mol) is essentially equal to that of electrostatic interactions (22.56 kcal/mol).

It is also apparent that the binding free energy for all simulated systems where the carrier is initially positioned adjacent to the major groove is similar to that for the minor groove, for example, 67.17 kcal/mol for 4⁺dendron–RNA complex initially adjacent to the major groove and 69.03 kcal/mol initially adjacent minor groove. The snapshots of Figure 2 provide a clue to this, since it is apparent that within the first 3 ns the dendron has already migrated to the major groove, even though it was initially located adjacent to the minor groove. Variations in the binding free energy for the two cases are therefore better ascribed to site specificity of the binding at different parts of the major groove along the strand.³²

The free energy for dissociation of the complexes can be derived directly from the binding free energies, as implied by the last row of Table 4 and Figure 8. The association process is exergonic with a favorable or negative free energy change, while the dissociation reaction is endergonic with an unfavorable or positive free energy change. Although the dissociation of the gene from the complex is a crucial step in gene delivery, the mechanism of gene release from the carrier systems is still not well understood. In our simulations, the dissociation free energies are the reverse of the binding free energies and are too strong to admit spontaneous dissociation of the gene–carrier complex in ideal solution. There are, however, many reports of cationic polymer gene delivery systems. The question arises naturally then: How does the gene release itself from the carrier–gene complex?

One possible factor may be that the ideal solution as explored here and the cytosolic fluid are fundamentally different in some way. In fact, the intracellular fluid is a crowded solution, with many different types of molecules filling much of the volume of a cell.⁷⁷ The concentration of macromolecules in the cytosol is extremely high, approximately in the range of 200–300 mg/mL, at which level they occupy a significant fraction (about 20–30%) of the total volume.⁷⁸ This high concentration of macromolecules in the cytoplasmic matrix causes an effect called macromolecular crowding—a term that encompasses the effects of excluded volume on the energetics and transport properties of macromolecules within a solution containing a high total volume fraction of macromolecules.⁷⁹ The crowding effect can greatly alter macromolecular reaction rates and equilibrium in the cytosol, especially dissociation constants by favoring the association of macromolecules.^{78,79} Previous studies indicated that cytosolic soluble proteins induce DNA release from DNA–cationic polymer complexes,^{80,81} and other studies showed

that the competitor DNA or RNA resulted in gene dissociation from the disassembly of the gene–polymer complex.^{82,83} Collectively, the implications of the binding and reverse dissociation free energies calculated in this work, together with the inferences of these experimental studies suggest that the mechanism of gene release within the cytosol is most probably the displacement of siRNA from the complex by negatively charged macromolecules in the cytosol. Further considerations along these lines, while intriguing, take us beyond the scope of the present modeling study and are reserved for later work.

4. Conclusions

The present simulations provide a detailed molecular level understanding of both structural and dynamical aspects of RNA–polycationic dendrimer complexation. All 4⁺ polymers preferentially migrate to and bind within the major groove regions of RNA, while 8⁺ polymers appear to bind less specifically on different sites of the RNA. The calculation of the binding free energy indicates that electrostatic attraction is the primary contributor to this interaction, followed by van der Waals forces. The binding free energy between 8⁺ polymer and RNA complex is higher than that of 4⁺ polymer. The structure of the polymer influences the nature and strength of its interaction with RNA. An overly strong interaction between the polycation and the nucleic acid will hamper the dissociation of the complex in the cytosol, and 4⁺ polymers may well be better in gene delivery than those analogues that are of considerably higher charge. Clearly, an important direction will be to carry out simulations for higher polycation/gene (\pm) charge ratios to reflect typical ratios used in experimental transfection studies, and such simulations are currently underway in our laboratory.

Acknowledgment. We acknowledge generous allocations of CPU time from the Australian National Computing Infrastructure (NCI) facility, the Computational Molecular Science Cluster Computing Facility at The University of Queensland, funded in part by the Australian Research Council (ARC) Linkage, Infrastructure, Equipment and Facilities (LIEF) scheme (Grant Number LE0882357), and the Deutsche Forschungsgemeinschaft (DFG, CellNetworks Cluster EC81).

Supporting Information Available: Chemical structures of six polymers (Figure S1), snapshots of 4+G0 and 4+linearlysine complexed with RNA (Figure S2), snapshots of 8+G0 and 8+linearlysine complexed with RNA (Figure S3), RMSD versus time of polymer-RNA complexation (Figure S4), variation of the number of contact points between 4+G0 or 8+G1 and DNA (Figure S5), variation of the number of contact points between 4+linearlysine or 8+linearlysine and DNA (Figure S6), number of water molecules in a spine of hydration (Figure S7), and snapshot of the complexation between 4+G0 and siRNA (Figure S8). This material is available free of charge via the Internet at <http://pubs.acs.org>.

References and Notes

- Niidome, T.; Huang, L. Gene therapy progress and prospects: nonviral vectors. *Gene Ther.* **2002**, *9* (24), 1647–1652.
- Pouton, C. W.; Seymour, L. W. Key issues in non-viral gene delivery. *Adv. Drug Delivery Rev.* **2001**, *46* (1–3), 187–203.
- Roth, C. M.; Sundaram, S. Engineering synthetic vectors for improved DNA delivery: Insights from intracellular pathways. *Annu. Rev. Biomed. Eng.* **2004**, *6*, 397–426.
- Gersting, S. W.; Schillinger, U.; Lausier, J.; Nicklaus, P.; Rudolph, C.; Plank, C.; Reinhardt, D.; Rosemeyer, J. Gene delivery to respiratory epithelial cells by magnetofection. *J. Gene Med.* **2004**, *6* (8), 913–922.
- Ruponen, M.; Honkakoski, P.; Ronkko, S.; Pelkonen, J.; Tammi, M.; Urtti, A. Extracellular and intracellular barriers in non-viral gene delivery. *J. Controlled Release* **2003**, *93* (2), 213–217.
- Zabner, J.; Fasbender, A. J.; Moninger, T.; Poellinger, K. A.; Welsh, M. J. Cellular and molecular barriers to gene transfer by a cationic lipid. *J. Biol. Chem.* **1995**, *270* (32), 18997–19007.
- Schaffer, D. V.; Fidelman, N. A.; Dan, N.; Lauffenburger, D. A. Vector unpacking as a potential barrier for receptor-mediated polyplex gene delivery. *Biotechnol. Bioeng.* **2000**, *67* (5), 598–606.
- Yamagata, M.; Kawano, T.; Shiba, K.; Mori, T.; Katayama, Y.; Niidome, T. Structural advantage of dendritic poly(L-lysine) for gene delivery into cells. *Bioorg. Med. Chem.* **2007**, *15* (1), 526–532.
- Mannisto, M.; Vanderkerken, S.; Toncheva, V.; Elomaa, M.; Ruponen, M.; Schacht, E.; Urtti, A. Structure-activity relationships of poly(L-lysines): Effects of pegylation and molecular shape on physicochemical and biological properties in gene delivery. *J. Controlled Release* **2002**, *83* (1), 169–182.
- Bertschinger, M.; Backliwal, G.; Schertenleib, A.; Jordan, M.; Hacker, D. L.; Wurm, F. M. Disassembly of polyethylenimine-DNA particles in vitro: Implications for polyethylenimine-mediated DNA delivery. *J. Controlled Release* **2006**, *116* (1), 96–104.
- Jeong, G. J.; Byun, H. M.; Kim, J. M.; Yoon, H.; Choi, H. G.; Kim, W. K.; Kim, S. J.; Oh, Y. K. Biodistribution and tissue expression kinetics of plasmid DNA complexed with polyethylenimines of different molecular weight and structure. *J. Controlled Release* **2007**, *118* (1), 118–125.
- Kunath, K.; von Harpe, A.; Fischer, D.; Peterson, H.; Bickel, U.; Voigt, K.; Kissel, T. Low-molecular-weight polyethylenimine as a non-viral vector for DNA delivery: Comparison of physicochemical properties, transfection efficiency and in vivo distribution with high-molecular-weight polyethylenimine. *J. Controlled Release* **2003**, *89* (1), 113–125.
- Kawakami, S.; Ito, Y.; Charoensit, P.; Yamashita, F.; Hashida, M. Evaluation of proinflammatory cytokine production induced by linear and branched polyethylenimine/plasmid DNA complexes in mice. *J. Pharmacol. Exp. Ther.* **2006**, *317* (3), 1382–1390.
- Brissault, B.; Leborgne, C.; Guis, C.; Danos, O.; Cheradame, H.; Kichler, A. Linear topology confers *in vivo* gene transfer activity to polyethylenimines. *Bioconjugate Chem.* **2006**, *17* (3), 759–765.
- Wightman, L.; Kircheis, R.; Rossler, V.; Carotta, S.; Ruzicka, R.; Kursa, M.; Wagner, E. Different behavior of branched and linear polyethylenimine for gene delivery in vitro and in vivo. *J. Gene Med.* **2001**, *3* (4), 362–372.
- Jones, N. A.; Hill, I. R. C.; Stolnik, S.; Bignotti, F.; Davis, S. S.; Garnett, M. C. Polymer chemical structure is a key determinant of physicochemical and colloidal properties of polymer-DNA complexes for gene delivery. *Biochim. Biophys. Acta, Gene Struct. Express.* **2000**, *1517* (1), 1–18.
- Lee, C. C.; Liu, Y.; Reineke, T. M. General structure-activity relationship for poly(glycamidoamine)s: The effect of amine density on cytotoxicity and DNA delivery efficiency. *Bioconjugate Chem.* **2008**, *19* (2), 428–440.
- Hsu, C. Y. M.; Uludag, H. Effects of size and topology of DNA molecules on intracellular delivery with non-viral gene carriers. *BMC Biotechnol.* **2008**, *8*.
- Parekh, H. S.; Marano, R. J.; Rakoczy, E. P.; Blanchfield, J.; Toth, I. Synthesis of a library of polycationic lipid core dendrimers and their evaluation in the delivery of an oligonucleotide with hVEGF inhibition. *Bioorg. Med. Chem.* **2006**, *14* (14), 4775–4780.
- Parekh, H. S. The advance of dendrimers—A versatile targeting platform for gene/drug delivery. *Curr. Pharm. Des.* **2007**, *13* (27), 2837–2850.
- Mann, A.; Richa, R.; Ganguli, M. DNA condensation by poly-L-lysine at the single molecule level: Role of DNA concentration and polymer length. *J. Controlled Release* **2008**, *125* (3), 252–262.
- Shen, X. C.; Zhou, J.; Liu, X.; Wu, J.; Qu, F.; Zhang, Z. L.; Pang, D. W.; Quelever, G.; Zhang, C. C.; Peng, L. Importance of size-to-charge ratio in construction of stable and uniform nanoscale RNA/dendrimer complexes. *Org. Biomol. Chem.* **2007**, *5* (22), 3674–3681.
- Van Rompaey, E.; Chen, Y.; Muller, J. D.; Gratton, E.; Van Craenenbroeck, E.; Engelborghs, Y.; De Smedt, S.; Demeester, J. Fluorescence fluctuation analysis for the study of interactions between oligonucleotides and polycationic polymers. *Biol. Chem.* **2001**, *382* (3), 379–386.
- Margineanu, A.; De Feyter, S.; Melnikov, S.; Marchand, D.; van Aerschot, A.; Herdewijn, P.; Habuchi, S.; De Schryver, F. C.; Hofkens, J. Complexation of lipofectamine and cholesterol-modified DNA sequences studied by single-molecule fluorescence techniques. *Biomacromolecules* **2007**, *8* (11), 3382–3392.
- Lucas, B.; Van Rompaey, E.; De Smedt, S. C.; Demeester, J.; Van Oostveldt, P. Dual-color fluorescence fluctuation spectroscopy to study the complexation between poly-L-lysine and oligonucleotides. *Macromolecules* **2002**, *35* (21), 8152–8160.

- (26) Lyulin, S. V.; Darinskii, A. A.; Lyulin, A. V. Computer simulation of complexes of dendrimers with linear polyelectrolytes. *Macromolecules* **2005**, *38* (9), 3990–3998.
- (27) Lyulin, S. V.; Vattulainen, I.; Gurtovenko, A. A. Complexes comprised of charged dendrimers, linear polyelectrolytes, and counterions: Insight through coarse-grained molecular dynamics simulations. *Macromolecules* **2008**, *41* (13), 4961–4968.
- (28) Farago, O.; Gronbech-Jensen, N. Computational and analytical modeling of cationic lipid-DNA complexes. *Biophys. J.* **2007**, *92* (9), 3228–3240.
- (29) Farago, O.; Ewert, K.; Ahmad, A.; Evans, H. M.; Gronbech-Jensen, N.; Safinya, C. R. Transitions between distinct compaction regimes in complexes of multivalent cationic lipids and DNA. *Biophys. J.* **2008**, *95* (2), 836–846.
- (30) Thyveetil, M. A.; Coveney, P. V.; Greenwell, H. C.; Suter, J. L. Role of host layer flexibility in DNA guest intercalation revealed by computer simulation of layered nanomaterials. *J. Am. Chem. Soc.* **2008**, *130* (37), 12485–12495.
- (31) Thyveetil, M. A.; Coveney, P. V.; Greenwell, H. C.; Suter, J. L. Computer simulation study of the structural stability and materials properties of DNA-intercalated layered double hydroxides. *J. Am. Chem. Soc.* **2008**, *130* (14), 4742–4756.
- (32) Maiti, P. K.; Bagchi, B. Structure and dynamics of DNA-dendrimer complexation: Role of counterions, water, and base pair sequence. *Nano Lett.* **2006**, *6* (11), 2478–2485.
- (33) Nikakhtar, A.; Nasehzadeh, A.; Mansoori, G. A. Formation and stability conditions of DNA-dendrimer nano-clusters. *J. Comput. Theor. Nanosci.* **2007**, *4* (3), 521–528.
- (34) Bandyopadhyay, S.; Tarek, M.; Klein, M. L. Molecular dynamics study of a lipid-DNA complex. *J. Phys. Chem. B* **1999**, *103* (46), 10075–10080.
- (35) Molas, M.; Bartrons, R.; Perales, J. C. Single-stranded DNA condensed with poly-L-lysine results in nanometric particles that are significantly smaller, more stable in physiological ionic strength fluids and afford higher efficiency of gene delivery than their double-stranded counterparts. *Biochim. Biophys. Acta, Gen. Subj.* **2002**, *1572* (1), 37–44.
- (36) Pavan, G. M.; Danani, A.; Pricl, S.; Smith, D. K. Modeling the multivalent recognition between dendritic molecules and DNA: Understanding how ligand “sacrifice” and screening can enhance binding. *J. Am. Chem. Soc.* **2009**, *131* (28), 9686–9694.
- (37) Srinivasan, J.; Cheatham, T. E.; Cieplak, P.; Kollman, P. A.; Case, D. A. Continuum solvent studies of the stability of DNA, RNA, and phosphoramidate–DNA helices. *J. Am. Chem. Soc.* **1998**, *120* (37), 9401–9409.
- (38) Kollman, P. A.; Massova, I.; Reyes, C.; Kuhn, B.; Huo, S. H.; Chong, L.; Lee, M.; Lee, T.; Duan, Y.; Wang, W.; Donini, O.; Cieplak, P.; Srinivasan, J.; Case, D. A.; Cheatham, T. E. Calculating structures and free energies of complex molecules: Combining molecular mechanics and continuum models. *Acc. Chem. Res.* **2000**, *33* (12), 889–897.
- (39) Kuhn, B.; Kollman, P. A. Binding of a diverse set of ligands to avidin and streptavidin: An accurate quantitative prediction of their relative affinities by a combination of molecular mechanics and continuum solvent models. *J. Med. Chem.* **2000**, *43* (20), 3786–3791.
- (40) Lee, M. R.; Duan, Y.; Kollman, P. A. Use of MM-PB/SA in estimating the free energies of proteins: Application to native, intermediates, and unfolded villin headpiece. *Proteins: Struct., Funct., Genet.* **2000**, *39* (4), 309–316.
- (41) Massova, I.; Kollman, P. A. Combined molecular mechanical and continuum solvent approach (MM-PBSA/GBSA) to predict ligand binding. *Perspect. Drug Discovery Des.* **2000**, *18*, 113–135.
- (42) Reyes, C. M.; Kollman, P. A. Structure and thermodynamics of RNA-protein binding: Using molecular dynamics and free energy analyses to calculate the free energies of binding and conformational change. *J. Mol. Biol.* **2000**, *297* (5), 1145–1158.
- (43) Case, D. A.; Darden, T. A.; Cheatham, I. T. E.; Simmerling, C. L.; Wang, J.; Duke, R. E.; Luo, R.; Merz, K. M.; Pearlman, D. A.; Crowley, M.; Walker, R. C.; Zhang, W.; Wang, B.; Hayik, S.; Roitberg, A.; Seabra, G.; Wong, K. F.; Paesani, F.; Wu, X.; Brozell, S.; Tsui, V.; Gohlke, H.; Yang, L.; Tan, C.; Mongan, J.; Hornak, V.; Cui, G.; Beroza, P.; Mathews, D. H.; Schafmeister, C.; Ross, W. S.; Kollman, P. A. AMBER 9; University of California: San Francisco, 2006.
- (44) Case, D. A.; Cheatham, T. E.; Darden, T.; Gohlke, H.; Luo, R.; Merz, K. M.; Onufriev, A.; Simmerling, C.; Wang, B.; Woods, R. J. The Amber biomolecular simulation programs. *J. Comput. Chem.* **2005**, *26* (16), 1668–1688.
- (45) Pearlman, D. A.; Case, D. A.; Caldwell, J. W.; Ross, W. S.; Cheatham, T. E.; Debolt, S.; Ferguson, D.; Seibel, G.; Kollman, P. AMBER, a package of computer-programs for applying molecular mechanics, normal-mode analysis, molecular-dynamics and free-energy calculations to simulate the structural and energetic properties of molecules. *Comput. Phys. Commun.* **1995**, *91* (1–3), 1–41.
- (46) Putral, L. N.; Bywater, M. J.; Gu, W.; Saunders, N. A.; Gabrielli, B. G.; Leggatt, G. R.; McMillan, N. A. RNA interference against human papillomavirus oncogenes in cervical cancer cells results in increased sensitivity to cisplatin. *Mol. Pharmacol.* **2005**, *68* (5), 1311–1319.
- (47) Wang, J. M.; Cieplak, P.; Kollman, P. A. How well does a restrained electrostatic potential (RESP) model perform in calculating conformational energies of organic and biological molecules. *J. Comput. Chem.* **2000**, *21* (12), 1049–1074.
- (48) Wang, J. M.; Wolf, R. M.; Caldwell, J. W.; Kollman, P. A.; Case, D. A. Development and testing of a general amber force field (vol 25, pg 1157, 2004). *J. Comput. Chem.* **2005**, *26* (1), 114–114.
- (49) Darden, T.; York, D.; Pedersen, L. Particle mesh Ewald—An N.Log(N) method for Ewald sums in large systems. *J. Chem. Phys.* **1993**, *98* (12), 10089–10092.
- (50) Essmann, U.; Perera, L.; Berkowitz, M. L.; Darden, T.; Lee, H.; Pedersen, L. G. A smooth particle mesh Ewald method. *J. Chem. Phys.* **1995**, *103* (19), 8577–8593.
- (51) Crowley, M. F.; Darden, T. A.; Cheatham, T. E.; Deerfield, D. W. Adventures in improving the scaling and accuracy of a parallel molecular dynamics program. *J. Supercomputing* **1997**, *11* (3), 255–278.
- (52) Sagui, C.; Darden, T. A. In *P3M and PME: a Comparison of the Two Methods*, Workshop on Treatment of Electrostatic Interactions in Computer Simulations of Condensed Media, Santa Fe, NM, Jun 23–25; Pratt, L. R., Hummer, G., Eds.; Amer. Inst. Physics: Melville, NY, 1999; pp 104–113.
- (53) Toukmaji, A.; Sagui, C.; Board, J.; Darden, T. Efficient particle-mesh Ewald based approach to fixed and induced dipolar interactions. *J. Chem. Phys.* **2000**, *113* (24), 10913–10927.
- (54) Sagui, C.; Pedersen, L. G.; Darden, T. A. Towards an accurate representation of electrostatics in classical force fields: Efficient implementation of multipolar interactions in biomolecular simulations. *J. Chem. Phys.* **2004**, *120* (1), 73–87.
- (55) Jorgensen, W. L.; Chandrasekhar, J.; Madura, J. D.; Impey, R. W.; Klein, M. L. Comparison of simple potential functions for simulating liquid water. *J. Chem. Phys.* **1983**, *79* (2), 926–935.
- (56) Leach, A. R. *Molecular Modelling: Principles and Applications*, 2nd ed.; Prentice Hall: New York, 2001.
- (57) Hötje, H.-D.; Sippl, W.; Rogan, D.; Folkers, G. *Molecular Modeling: Basic Principles and Applications*, 3rd ed.; Wiley-VCH: Weinheim, 2008.
- (58) Ryckaert, J. P.; Cicotti, G.; Berendsen, H. J. C. Numerical integration of Cartesian equations of motion of a system with constraints—Molecular-dynamics of *n*-alkanes. *J. Comput. Phys.* **1977**, *23* (3), 327–341.
- (59) Cerutti, D. S.; Duke, R.; Freddolino, P. L.; Fan, H.; Lybrand, T. P. A vulnerability in popular molecular dynamics packages concerning Langevin and Andersen dynamics. *J. Chem. Theory Comput.* **2008**, *4* (10), 1669–1680.
- (60) Berendsen, H. J. C.; Postma, J. P. M.; Vangunsteren, W. F.; Dinola, A.; Haak, J. R. Molecular-dynamics with coupling to an external bath. *J. Chem. Phys.* **1984**, *81* (8), 3684–3690.
- (61) Wu, X. W.; Brooks, B. R. Self-guided Langevin dynamics simulation method. *Chem. Phys. Lett.* **2003**, *381* (3–4), 512–518.
- (62) Luo, R.; David, L.; Gilson, M. K. Accelerated Poisson-Boltzmann calculations for static and dynamic systems. *J. Comput. Chem.* **2002**, *23* (13), 1244–1253.
- (63) Lu, Q.; Luo, R. A Poisson-Boltzmann dynamics method with nonperiodic boundary condition. *J. Chem. Phys.* **2003**, *119* (21), 11035–11047.
- (64) Honig, B.; Nicholls, A. Classical electrostatics in biology and chemistry. *Science* **1995**, *268* (5214), 1144–1149.
- (65) Still, W. C.; Tempczyk, A.; Hawley, R. C.; Hendrickson, T. Semianalytical treatment of solvation for molecular mechanics and dynamics. *J. Am. Chem. Soc.* **1990**, *112* (16), 6127–6129.
- (66) Jayaram, B.; Sprous, D.; Beveridge, D. L. Solvation free energy of macromolecules: Parameters for a modified generalized born model consistent with the AMBER force field. *J. Phys. Chem. B* **1998**, *102* (47), 9571–9576.
- (67) Cramer, C. J.; Truhlar, D. G. Implicit solvation models: Equilibria, structure, spectra, and dynamics. *Chem. Rev.* **1999**, *99* (8), 2161–2200.
- (68) Bashford, D.; Case, D. A. Generalized born models of macromolecular solvation effects. *Annu. Rev. Phys. Chem.* **2000**, *51*, 129–152.
- (69) Onufriev, A.; Bashford, D.; Case, D. A. Modification of the generalized Born model suitable for macromolecules. *J. Phys. Chem. B* **2000**, *104* (15), 3712–3720.
- (70) Lee, M. S.; Salsbury, F. R.; Brooks, C. L. Novel generalized Born methods. *J. Chem. Phys.* **2002**, *116* (24), 10606–10614.
- (71) AMBER. AMBER 9 Users’ Manual; <http://ambermd.org/doc9/>.
- (72) Cornell, W. D.; Cieplak, P.; Bayly, C. I.; Gould, I. R.; Merz, K. M.; Ferguson, D. M.; Spellmeyer, D. C.; Fox, T.; Caldwell, J. W.; Kollman, P. A. A 2nd generation force-field for the simulation of proteins, nucleic-acids, and organic-molecules. *J. Am. Chem. Soc.* **1995**, *117* (19), 5179–5197.

- (73) Sitkoff, D.; Sharp, K. A.; Honig, B. Accurate calculation of hydration free-energies using macroscopic solvent models. *J. Phys. Chem. US* **1994**, *98* (7), 1978–1988.
- (74) Connolly, M. L. Analytical molecular-surface calculation. *J. Appl. Crystallogr.* **1983**, *16*, 548–558.
- (75) Ouyang, D. F.; Zhang, H.; Herten, D. P.; Parekh, H. S.; Smith, S. C. Flexibility of short-strand RNA in aqueous solution as revealed by molecular dynamics simulation: Are A-RNA and A'-RNA distinct conformational structures. *Aust. J. Chem.* **2009**, *62* (9), 1054–1061.
- (76) Lu, X. J.; Olson, W. K. 3DNA: A software package for the analysis, rebuilding and visualization of three-dimensional nucleic acid structures. *Nucleic Acids Res.* **2003**, *31* (17), 5108–5121.
- (77) Goodsell, D. S. Inside a living cell. *Trends Biochem. Sci.* **1991**, *16* (6), 203–206.
- (78) Ellis, R. J. Macromolecular crowding: Obvious but underappreciated. *Trends Biochem. Sci.* **2001**, *26* (10), 597–604.
- (79) Zhou, H. X.; Rivas, G. N.; Minton, A. P. Macromolecular crowding and confinement: Biochemical, biophysical, and potential physiological consequences. *Annu. Rev. Biophys.* **2008**, *37*, 375–397.
- (80) Okuda, T.; Niidome, T.; Aoyagi, H. Cytosolic soluble proteins induce DNA release from DNA-gene carrier complexes. *J. Controlled Release* **2004**, *98* (2), 325–332.
- (81) Iida, T.; Mori, T.; Katayama, Y.; Niidome, T. Overall interaction of cytosolic proteins with the PEI/DNA complex. *J. Controlled Release* **2007**, *118* (3), 364–369.
- (82) Bertschinger, M.; Backliwal, G.; Schertenleib, A.; Jordan, M.; Hacker, D. L.; Wurm, F. M. Disassembly of polyethylenimine-DNA particles in vitro: Implications for polyethylenimine-mediated DNA delivery. *J. Controlled Release* **2006**, *116* (1), 96–104.
- (83) Huth, S.; Hoffmann, F.; von Gersdorff, K.; Laner, A.; Reinhardt, D.; Rosencker, J.; Rudolph, C. Interaction of polyamine gene vectors with RNA leads to the dissociation of plasmid DNA-carrier complexes. *J. Gene Med.* **2006**, *8* (12), 1416–1424.
- (84) Ward, C. M.; Read, M. L.; Seymour, L. W. Systemic circulation of poly(L-lysine)/DNA vectors is influenced by polycation molecular weight and type of DNA: Differential circulation in mice and rats and the implications for human gene therapy. *Blood* **2001**, *97* (8), 2221–2229.

JP911906E